

Observation of the second ${}^3\Pi_u$ valence state of O_2

B. R. Lewis, P. M. Dooley, J. P. England, K. Waring, S. T. Gibson, and K. G. H. Baldwin
*Research School of Physical Sciences and Engineering, The Australian National University,
 Canberra, Australian Capital Territory 0200, Australia*

H. Partridge

NASA Ames Research Center, Moffett Field, California 94035

(Received 15 July 1996)

Rotational perturbations in the $B\ {}^3\Sigma_u^-$ state of molecular oxygen are studied by measuring high-resolution vacuum ultraviolet laser photoabsorption cross sections of the (16,0)–(18,0) $B\ {}^3\Sigma_u^- \leftarrow X\ {}^3\Sigma_g^-$ Schumann-Runge bands of ${}^{16}\text{O}_2$. The observation of numerous extra lines in the spectrum, together with *ab initio* calculations of relevant potential-energy curves, enables the perturbing state to be assigned as the second valence state of ${}^3\Pi_u$ symmetry. This weakly bound state, which we name $C'\ {}^3\Pi_u$, is also likely to be principally responsible for the well-known rapid increase in the magnitudes of the B -state triplet-splitting constants λ_v and γ_v as the dissociation limit is approached. [S1050-2947(96)07911-5]

PACS number(s): 33.20.Ni, 33.70.Jg

I. INTRODUCTION

Molecular oxygen plays an important role in the photochemistry of the terrestrial atmosphere through its absorption of solar vacuum ultraviolet (VUV) radiation and subsequent (pre)dissociation. In particular, a precise knowledge of the spectroscopic parameters, oscillator strengths, and predissociation linewidths of the Schumann-Runge (SR) system, $B\ {}^3\Sigma_u^- \leftarrow X\ {}^3\Sigma_g^-$ is necessary for realistic photochemical modeling of the stratosphere and mesosphere [1,2].

The SR bands of O_2 have been the subject of much study. The many spectroscopic investigations have been reviewed by Yoshino *et al.* [3], while Lewis *et al.* [4] have recently reviewed work on the $B\ {}^3\Sigma_u^-$ -state predissociation. The B state is subject to a number of perturbations. Relevant potential-energy curves are shown in Fig. 1, where the $B\ {}^3\Sigma_u^-$ curve is a Rydberg-Klein-Rees (RKR) potential determined by Lewis *et al.* [5] and the repulsive curves are the *ab initio* calculations of Partridge *et al.* [6] ($1\ {}^3\Pi_u$, $1\ {}^5\Pi_u$) and Partridge [7] ($1\ {}^1\Pi_u$, $2\ {}^3\Sigma_u^+$). As has been shown by Julienne and Krauss [8] and Julienne [9], the four repulsive states in Fig. 1 are responsible for the predissociation of every vibrational level of the B state and are also expected to produce irregular perturbations in the spectroscopic and triplet-splitting constants of the B state. In particular, the $1\ {}^3\Pi_u$ state is expected to perturb G_v , B_v , λ_v , and γ_v through a combination of spin-orbit, spin-electronic, and L-uncoupling interactions. Irregular perturbations have indeed been observed in the second vibrational differences $\Delta^2 G_v$ of the B state for $v=1-10$ and can be explained using the same model as that necessary to explain the observed predissociation [4,8,10].

In addition to the perturbations of the B -state vibrational structure caused by the repulsive states in Fig. 1, perturbations in the rotational structure of the B state have been observed for $v \geq 16$ in every O_2 isotopomer studied [3,10–12]. A few extra levels associated with the bound perturbing state(s) have been reported [3,11], but the level assignments

are tentative, the perturbations remain unanalyzed, and no progress has been made in the identification of the perturbing state. Finally, for all O_2 isotopomers studied, the triplet-splitting constants λ_v and γ_v for $B\ {}^3\Sigma_u^-$ ($v \geq 11$) exhibit rapidly increasing smooth perturbations as the dissociation limit is approached [10]. Bergeman and Wofsy [13], using the unique-perturber approximation of Zare *et al.* [14], have invoked a spin-orbit interaction between the $B\ {}^3\Sigma_u^-$ state and a ${}^3\Pi_u$ state correlating with the $\text{O}({}^1D) + \text{O}({}^3P)$ dissociation limit to explain this observed perturbation in λ_v . A similar approach has been followed by Cheung *et al.* [10], without assignment of the perturber.

In this work, we measure high-resolution photoabsorption cross sections for selected rotational lines from the (16,0)–(18,0) SR bands of ${}^{16}\text{O}_2$ and observe consistent sets of extra lines associated with the lowest-energy rotational perturbations of the F_2 levels of $B\ {}^3\Sigma_u^-$ ($v=16-18$). In addition, we perform *ab initio* calculations of possible perturbing states. A

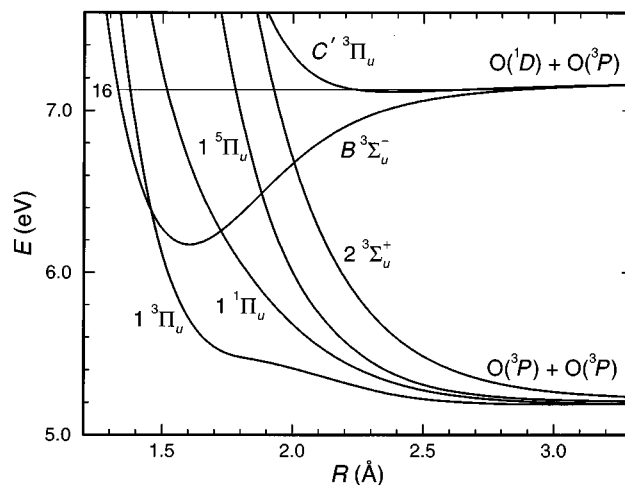


FIG. 1. Potential-energy curves for electronic states of O_2 relevant to perturbation of the $B\ {}^3\Sigma_u^-$ state. Energies are given relative to the minimum of the ground-state $X\ {}^3\Sigma_g^-$ potential-energy curve.

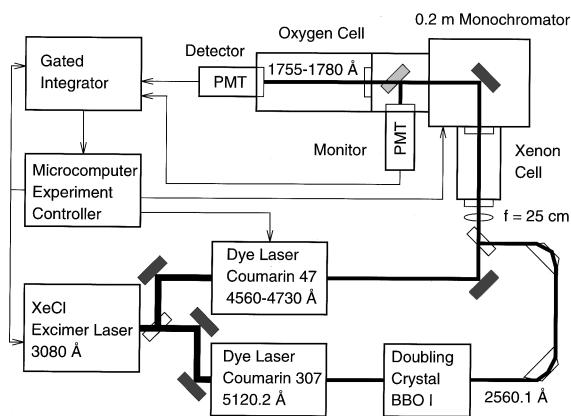


FIG. 2. Schematic diagram of the experimental apparatus.

full characterization of the perturbations, together with the *ab initio* calculations, leads to an assignment of the perturbing state as the second valence state of ${}^3\Pi_u$ symmetry, which we name $C' {}^3\Pi_u$. The calculated potential-energy curve for this state is shown in Fig. 1, where it can be seen that the $C' {}^3\Pi_u$ state is bound for energies near $B {}^3\Sigma_u^-(v \geq 16)$. In addition, we show that the C' state is also likely to be principally responsible for the rapidly increasing smooth perturbations observed in the B -state triplet-splitting constants λ_v and γ_v .

II. EXPERIMENTAL METHOD

The experimental apparatus, shown schematically in Fig. 2, is similar to that used in an earlier study of the $f' {}^1\Sigma_u^+$ and $f' {}^1\Sigma_u^+$ states of O_2 and described in detail elsewhere [15]. Briefly, we used two-photon-resonant difference-frequency four-wave mixing (2PR-4WDM) in Xe [16,17] to generate narrow-bandwidth, tunable vacuum ultraviolet radiation in the range 1755–1780 Å in order to study rotational perturbations in $B {}^3\Sigma_u^-(v = 16-18)$ by means of high-resolution photoabsorption spectroscopy.

One of the excimer-pumped dye lasers (Coumarin 307 in methanol) was tuned to a vacuum wavelength of 5120.2 Å so that its frequency-doubled output was two-photon resonant with the Xe transition $5p^5(2P_{3/2}^o)6p[\frac{5}{2}]_2 \leftarrow 5p^6 {}^1S_0$. The doubled radiation was combined, after removal of the fundamental radiation, with the tunable radiation from the other dye laser (Coumarin 47 in methanol) and both beams were focussed into a cell containing Xe (US Services Inc., 99.999%) by a 25-cm focal-length quartz lens. VUV radiation generated by the 2PR-4WDM process was passed through a 0.2-m VUV monochromator which acted as a broad bandpass filter, tuned synchronously with the second dye laser and discriminating against the fundamental and doubled dye-laser radiation. The VUV radiation leaving the exit slit of the monochromator was divided into two beams by a slotted Al beam splitter. The reflected beam was monitored directly, while the transmitted beam passed through a 33-cm long, MgF_2 -windowed absorption cell containing O_2 (BOC, 99.9%) before being detected. Output pulses from the solar-blind monitor and detector photomultipliers (EMI type 9413, CsI photocathode) were processed by a boxcar averaging system. A microcomputer was used to control the laser

and monochromator scanning, the pressure of O_2 in the absorption cell, and the acquisition of the shot-averaged detector and monitor signals from the boxcar system.

In order to obtain the measurements presented here, scans were performed at room temperature (293 K) over ~ 0.3 Å ranges in the VUV from $\sim 1755-1780$ Å with wavelength increments of 0.001 Å. The phase matching for each scan was optimized by adjusting the pressure of Xe in the range 70–90 Torr to maximize the VUV signal. The monitor and detector signals were averaged over 50 laser shots for each datum point, during groups of three scans with the absorption cell alternately filled with a pressure of O_2 in the range 0.8–15 Torr, then evacuated, then refilled. This scheme allowed compensation for any slow drifts in detector sensitivity and correction for wavelength dependences in the generated signal which were not related to O_2 absorption [15]. Division of the detector signal by the monitor signal, after correction for scattered radiation, provided a measure of compensation for the shot-to-shot fluctuations inherent in the generated VUV signal. Absolute cell transmittances were obtained by dividing the full-cell ratios [(detector)/(monitor)] by the empty-cell ratios for each wavelength. Photoabsorption cross sections were calculated from the absolute transmittances using the Beer-Lambert law. Statistical uncertainties in the measured (peak) cross sections were $\sim 3\%$ and there was an additional systematic uncertainty of $\sim 3\%$ arising from uncertainties in O_2 pressure, temperature, and cell length.

Each dye laser was operated with an intracavity etalon, resulting in a nominal bandwidth of 0.04 cm^{-1} full-width at half-maximum (FWHM) for each fundamental beam. The average VUV bandwidth was estimated to be $0.08 \pm 0.02 \text{ cm}^{-1}$ FWHM by fitting an instrumentally degraded Voigt profile to the SR lines of narrowest predissociation linewidth ($v' = 16, F_1, \text{high } N'$) [18]. This value is consistent with the bandwidth of $0.06 \pm 0.01 \text{ cm}^{-1}$ FWHM reported by Yamanouchi and Tsuchiya [17] for 2PR-4WDM in Sr vapor. The nominal VUV wave number was given by

$$\nu_{\text{vuv}} = \nu_{2p} - \nu_{\text{vis}}, \quad (1)$$

where ν_{2p} was the wave number of the Xe two-photon resonance and ν_{vis} was the vacuum-corrected wave number of the tunable dye laser. Absolute wave number calibration was achieved by comparison with the measured wave numbers of Yoshino *et al.* [3] for selected sharp, unblended lines of the SR system. The linearity and calibration of the dye-laser étalon scanning system were confirmed over the relatively small ($\leq 10 \text{ cm}^{-1}$) ranges involved, by comparison of the measured combination differences between SR lines having a common upper level with accurately known O_2 ground-state energy levels [19]. The estimated absolute uncertainty in the wave number of a sharp, unblended line is $\sim 0.1 \text{ cm}^{-1}$, while the relative uncertainty is $\sim 0.01-0.04 \text{ cm}^{-1}$, the smaller value applying in the case of two sharp lines within the one etalon scan.

III. LINE-PROFILE ANALYSIS

SR absorption-line wave numbers, oscillator strengths, and predissociation linewidths were determined by a least-

squares fitting procedure. In this procedure, the measured photoabsorption cross sections were compared with model calculations, appropriate to the experimental conditions, in which the line parameters were allowed to vary independently. For unperturbed lines, or for well separated pairs of perturbed lines, the predissociation component of the line shape was taken as Lorentzian. The corresponding cross section for the i th line was given by

$$\sigma_i(\nu) = \frac{0.563 \times 10^{-12} s_i}{\Gamma_i \left[1 + \left(\frac{\nu - \nu_i}{\Gamma_i/2} \right)^2 \right]} \text{ cm}^2, \quad (2)$$

where s_i is a strength factor related to the line oscillator strength, Γ_i (cm^{-1}) is the FWHM predissociation linewidth, and ν_i (cm^{-1}) is the wave number of the line center. As has been explained in detail elsewhere [20], Eq. (2) is inappropriate to describe the predissociation line shapes of perturbed pairs of lines whose separation does not greatly exceed their predissociation linewidths. In those cases, most noticeably for $v' = 16$, destructive interference was observed for wave numbers between the centers of the perturbed and perturbing lines, and, therefore, the i th pair of perturbed main (m) and extra (x) lines was described by the coupled predissociation line shape [20]

$$\sigma_i(\nu) = \frac{0.563 \times 10^{-12} s_i \left(\frac{\Gamma_m/2}{\nu - \nu_m} + \frac{\Gamma_x/2}{\nu - \nu_x} \right)^2}{\Gamma_i \left[1 + \left(\frac{\Gamma_m/2}{\nu - \nu_m} + \frac{\Gamma_x/2}{\nu - \nu_x} \right)^2 \right]} \text{ cm}^2, \quad (3)$$

where $\Gamma_i = \Gamma_m + \Gamma_x$ and s_i is the total strength for the pair of interfering lines. The Doppler component of the line shapes and the effects of the finite instrumental resolution were included in the model through appropriate convolution procedures and the underlying continuum was expressed as a low-order polynomial in ν .

IV. AB INITIO CALCULATIONS

The *ab initio* calculations followed the procedure reported in Ref. [6]. The orbitals were optimized using the state-averaged complete-active-space self-consistent-field (CASSCF) approach with the $2p$ orbitals active. The calculations were performed in D_{2h} symmetry with symmetry and equivalence restrictions imposed on the orbitals. All states of the specified spin and spatial symmetry which dissociate to the $\text{O}({}^3P) + \text{O}({}^3P)$ and $\text{O}({}^1D) + \text{O}({}^3P)$ asymptotes were included in the averaging; five states were included for the ${}^3\Pi_u$ (and ${}^3\Phi_u$) optimization and six were included for the ${}^3\Sigma_u^+$ and ${}^3\Delta_u$ states. External correlation was included using a multireference configuration-interaction (MRCI) procedure using the CASSCF reference and correlating both the $2s$ and $2p$ electrons. The effect of higher excitations was estimated using a multireference analog of the Davidson correction, denoted +Q. The basis set employed is the atomic natural orbitals (ANO) [21] basis set designated $[5s\ 4p\ (3+1)d\ 2f\ 1g] + (sp)$ [6]. The “+ sp ” indicates that the basis is augmented with diffuse s and p orbitals and the notation “ $(3+1)d$ ” indicates that there are three ANO

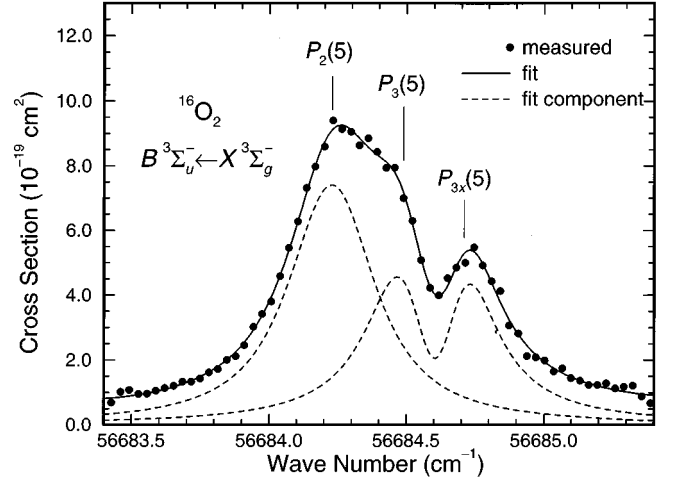


FIG. 3. Photoabsorption cross section for ${}^{16}\text{O}_2$ in the region of the $P_2(5)$ and $P_3(5)$ lines from the $(16,0)$ band of the $B\ {}^3\Sigma_u^- \leftarrow X\ {}^3\Sigma_g^-$ system, measured at $T=293$ K with an instrumental resolution of $\sim 0.06\ \text{cm}^{-1}$ FWHM. The fitted model cross section, and its components, which include the Doppler contribution, but not the instrumental degradation, are also shown. The $P_3(5)$ line is perturbed, a strong destructive interference being observed between the corresponding main and extra lines.

d functions and that the outer d primitive is uncontracted. This basis set provides an accurate description of the valence regions but does not contain the diffuse functions needed to describe Rydberg character. The potential-energy curves have not been corrected for basis-set superposition error (BSSE).

V. RESULTS AND DISCUSSION

A. Perturbations in $B\ {}^3\Sigma_u^-(v=16-18)$

A combination of high-resolution photoabsorption cross section measurements and the line-profile analysis technique described in Sec. III enabled the discovery and detailed characterization of many extra lines associated with rotational perturbations in $B\ {}^3\Sigma_u^-(v=16-18)$. It is usually not possible to obtain comparable information from spectrographic data alone, especially for blended spectral features, because of the difficulty in extracting reliable intensity information. In particular, we were able to measure the effects of the perturbations, not only on the term values, but also on the predissociation linewidths and oscillator strengths. Using this information, we were able to determine the J dependence of the perturbation matrix elements and thereby establish the symmetry of the perturbing state. While there are three fine-structure components associated with the $B\ {}^3\Sigma_u^-$ state, namely, the F_2 levels (f parity, $J=N$, $\Omega=1$) and the mixed F_1 and F_3 levels (e parity, $J=N\pm 1$, $\Omega=0$ and 1), the F_1 levels for $v=16-18$ are well separated from the F_2 and F_3 levels and do not participate in the particular perturbations discussed here.

As an example of an observed perturbation, in Fig. 3 we show the measured photoabsorption cross section in the region of the $P_2(5)$ and $P_3(5)$ lines from the $(16,0)$ SR band. It was not possible to obtain a convincing fit to the measured cross section when the predissociation line shapes of the

TABLE I. Wave numbers for main- (upper entries) and extra- (lower entries) branch lines from the $B^3\Sigma_u^-(v'=16, N', F_2 \text{ and } F_3) \leftarrow X^3\Sigma_g^-(v''=0, N'')$ band of $^{16}\text{O}_2$, together with upper-state term values, all in cm^{-1} . Absolute uncertainties $\sim 0.1 \text{ cm}^{-1}$, relative uncertainties $\sim 0.01-0.03 \text{ cm}^{-1}$.

N''	$R_2(N'')$ ^a	$P_2(N'')$	$R_3(N'')$	$P_3(N'')$	N'	$T_2(N')$ ^b	$T_3(N')$ ^b
1	56719.05 ^c				2	56721.88	56720.66
3	56710.07 ^c 56711.44 ^e	56704.65	56710.42 56710.65 ^d	56705.48 ^d	4	56727.37 56728.70	56725.60 56725.82
5	56692.80 ^d 56693.71	56684.23 ^c 56685.58 ^{c,e}	56693.32	56684.49 56684.71 ^d	6	56735.94 56736.85	56734.44
7	56666.87 56667.57 ^f	56655.43 56656.35	56667.85	56655.92	8	56747.39 56748.08	56746.38
9	56633.26 56632.12 ^{f,g}	56618.03 56618.74 ^{d,f}	56634.06	56619.00 ^c	10	56762.64 56761.49	56761.48
11	56590.64 56588.67	56572.94 56571.78 ^{f,g}	56591.89	56573.70	12	56780.33 56778.37	56779.66
13	56539.41 ^h	56518.82	56541.20	56520.05	14	56800.96	56800.82
15	56479.69	56456.19	56481.94	56457.91	16	56824.45	56824.85
17	56411.23	56384.96	56414.03	56387.20	18	56850.70	56851.63
19	56333.94	56305.10 ^h	56337.48 ^c	56307.84	20	56879.56	56881.21
21		56216.38		56219.87			

^aThe lines $^R Q_{21}(1)=56720.82 \text{ cm}^{-1}$, $^P Q_{23}(5)=56686.26 \text{ cm}^{-1}$, $^R Q_{32}(1)=56717.79 \text{ cm}^{-1}$, $^T R_{31}(1)=56724.60 \text{ cm}^{-1}$, and $^T R_{31x}(1)=56724.83 \text{ cm}^{-1}$ were also observed.

^bWeighted averages determined from the separate branch wave numbers.

^cBlended with a weaker line.

^dShoulder.

^eWeak.

^fExtra line also reported by Brix and Herzberg [11].

^gExtra line also reported by Yoshino *et al.* [3].

^hBlended with a stronger line.

three component lines were represented by Eq. (2). However, when the two higher-energy lines were described by Eq. (3), the excellent fit shown in Fig. 3 resulted. Evidently, the $P_3(5)$ line is split into two mutually-interfering components due to a perturbation. Although the shift in energy due to the perturbation is small, almost total intensity sharing occurs between the main and extra lines. This conclusion is confirmed following an analysis of our measured cross sections near the $R_3(3)$ and $^T R_{31}(1)$ lines which, together with $P_3(5)$, share the common upper level $N'=4, J'=3$. Our assignments [22], $P_2(5)=56\,684.23 \text{ cm}^{-1}$, $P_3(5)=56\,684.49 \text{ cm}^{-1}$ and $P_{3x}(5)=56\,684.71 \text{ cm}^{-1}$, differ from those of Brix and Herzberg [11] and Yoshino *et al.* [3], neither of whom report a perturbation for this level. Our measured cross section for the region near the $P_2(11)$ perturbation in the (16,0) band, which also exhibits a particularly obvious interference effect, has been reported elsewhere [20].

Wave numbers for the lines observed in this work, together with the corresponding upper-state term values, are summarized in Tables I–III. Where possible, the term values are averages of the values determined from the P - and R -branch wave numbers for unblended lines. Thirty-four ex-

tra lines have been observed, only four of which, to our knowledge, have been reported previously in spectrographic studies [3,11]. As mentioned in Sec. II, wave numbers for the main-branch lines in Tables I–III are calibrated against those of Yoshino *et al.* [3] and are essentially indistinguishable for unblended, sharp lines. However, the wave numbers in Tables I–III for the many blended features at lower rotation should be more reliable than those of Yoshino *et al.* [3] because of superior instrumental resolution and a realistic line-profile analysis procedure.

The term values in Tables I–III are presented in Fig. 4 in such a way as to emphasize the perturbed main and extra levels in the F_2 and F_3 fine-structure components. It can be seen clearly in Fig. 4 that the F_2 levels for $v=16-18$ are perturbed by levels with smaller rotational constants. However, these perturbations fall into two classes. First, through the observation of the single extra level associated with the F_3 perturbation for $v=16, J=3$, it is apparent that the corresponding perturbing level has closely spaced e - and f -parity components, implying a perturbing state with $\Lambda \geq 1$ and a very small Λ doubling. Second, in contrast, the F_3 levels for $v=17$ and 18 are unperturbed in the range of rotation under consideration, implying that the F_2 -level per-

TABLE II. Wave numbers for main- (upper entries) and extra- (lower entries) branch lines from the $B\ {}^3\Sigma_u^-(v'=17, N', F_2 \text{ and } F_3) \leftarrow X\ {}^3\Sigma_g^-(v''=0, N'')$ band of ${}^{16}O_2$, together with upper-state term values, all in cm^{-1} . Absolute uncertainties $\sim 0.1\ cm^{-1}$, relative uncertainties $\sim 0.04\ cm^{-1}$.

N''	$R_2(N'')$	$P_2(N'')$	$R_3(N'')$	$P_3(N'')$	N'	$T_2(N')^a$	$T_3(N')^a$
1	56851.62				2	56854.50	56853.29
3	56842.11	56837.29 ^b	56842.62 ^b	56838.12	4	56859.35	56857.79
5	56823.78	56816.22	56824.25 ^b	56816.67 ^c	6	56866.92	56865.41
7	56796.63	56786.41	56797.44	56786.88	8	56877.16	56875.98
9	56760.69	56747.80	56761.96	56748.57	10	56890.06	56889.38
11	56715.78	56700.42 ^d	56717.67 ^b	56701.61	12	56905.49	56905.43
13	56661.94	56643.99	56664.48	56645.83	14	56923.42	56924.09
15	56598.82 ^b 56606.92	56578.63	56602.28	56581.16	16	56943.56 56951.68	56945.21
17		56504.09	56530.89	56507.54 ^b	18	56965.59 56971.36	56968.51
19	56448.56 ^{b,c} 56443.11 ^e	56419.98		56424.72 ^c	20	56994.17 56988.72	
21	56357.03 ^d 56349.59	56330.99 ^d 56325.57 ^d			22	57020.22 57012.74	
23	56256.58	56228.09 56220.58			24	57048.69 57038.04	
25	56146.56 56132.52	56116.21 56105.58			26	57079.02 57064.96	
27		55980.81					

^aWeighted averages determined from the separate branch wave numbers.

^bBlended with a weaker line.

^cShoulder.

^dBlended with a stronger line.

^eAssignment differs from that of Yoshino *et al.* [3].

turber is either a Σ state, or a state with $\Lambda \geq 1$ and a very large Λ doubling.

The measured cross sections for perturbed pairs of lines from the (16,0) band were fitted using Eq. (3), allowing the determination of separate predissociation linewidths for the main and extra lines and the corresponding line-strength sums. These data are presented in Table IV as Γ_x/Γ_m , $\Gamma_x + \Gamma_m$, and $f_{v'm} + f_{v'i} (=f_{v'i})$. The line strengths have been converted into equivalent band oscillator strengths using the relation

$$f_{v'i} = s_i / (\alpha_i'' S_i), \quad (4)$$

where α_i'' and S_i are appropriately normalized Boltzmann and Hönl-London factors, respectively. For the (17,0) and (18,0) bands, where Eq. (2) was used to fit the measured cross sections, linewidth and oscillator-strength ratios were determined independently and the weighted average of these ratios is given in the Γ_x/Γ_m column of Table IV. Where possible, the data listed in Table IV were determined as

weighted averages of separate P - and R -branch measurements. Predissociation linewidths and oscillator strengths are also shown in Figs. 5 and 6, respectively, for the F_2 main lines from the (16,0)–(18,0) bands, together with the corresponding main-extra sums. The effects of the perturbations on the main-line parameters are clearly evident. It is also apparent from Figs. 5 and 6 that the predissociation-linewidth and oscillator-strength sums in the perturbed regions join smoothly onto the values for the unperturbed levels. These observations confirm the validity of the two assumptions implicit in the use of Eq. (3): in the absence of perturbations, levels of the perturbing state are not predissociated and transitions into them from the ground state have insignificant strength [20]. With these assumptions, the measured term-value separations $\Delta T = |T_m - T_x|$ and predissociation-linewidth ratios $r = \Gamma_x/\Gamma_m (=f_{v'x}/f_{v'm})$ for the main- and extra-level pairs in Table IV can be used to calculate perturbation matrix elements and level shifts. Within the framework of standard two-level perturbation theory [23], it is easy to show that the perturbation matrix element is given by

TABLE III. Wave numbers for main- (upper entries) and extra- (lower entries) branch lines from the $B^3\Sigma_u^-(v'=18, N', F_2 \text{ and } F_3) \leftarrow X^3\Sigma_g^-(v''=0, N'')$ band of $^{16}\text{O}_2$, together with upper-state term values, all in cm^{-1} . Absolute uncertainties $\sim 0.1 \text{ cm}^{-1}$, relative uncertainties $\sim 0.04 \text{ cm}^{-1}$.

N''	$R_2(N'')$ ^a	$P_2(N'')$	$R_3(N'')$	$P_3(N'')$	N'	$T_2(N')$ ^b	$T_3(N')$ ^b
1	56953.52				2	56956.40	56955.40
3	56943.24 56948.55 ^d	56939.15	56943.96 ^c	56940.23	4	56960.48 56965.80	56959.16
5	56923.66 ^e 56928.34 ^c	56917.38 ^e 56922.67 ^d	56924.53	56918.05	6	56966.80 56971.53	56965.64
7	56894.65 56898.98	56886.29 56891.02	56896.18	56887.11	8	56975.15 56979.48	56974.71
9	56856.01 56860.53	56845.77 56850.10	56858.79	56847.28 ^e	10	56985.35 56989.90	56986.21
11	56813.03 56807.62 ^e	56795.62 56800.20 ^e	56812.03 ^e	56798.38 ^c	12	57002.73 56997.32	56999.78
13	56756.44 56749.66	56741.19 ^c 56735.82		56740.18	14	57017.94 57011.16	
15		56673.15 ^e 56666.38					

^aThe lines $^R Q_{32}(1) = 56952.52 \text{ cm}^{-1}$ and $^T R_{31}(3) = 56950.35 \text{ cm}^{-1}$ were also observed.

^bWeighted averages determined from the separate branch wave numbers.

^cBlended with a stronger line.

^dWeak.

^eBlended with a weaker line.

$$|H_{mx}| = \sqrt{r\Delta T/(1+r)}, \quad (5)$$

and the magnitude of the level shift by

$$|S| = r\Delta T/(1+r). \quad (6)$$

Values calculated using Eqs. (5) and (6) are included in Table IV and the perturbation matrix elements are also shown in Fig. 7. It is clear from Fig. 7 that the F_2 matrix elements for $v=16-18$ exhibit an essentially linear dependence on rotation and that the single F_3 perturbation matrix element for $v=16, J=3$ lies marginally below the line representing the $v=16, F_2$ data. These are key observations which help to determine the symmetry of the perturbing state.

The heterogeneous nature of the F_2 -level perturbations shown in Fig. 7 ($\Delta\Omega = \pm 1$) confirms that the perturbing state is of *ungerade* symmetry with $\Omega=0$ or 2. If each perturbation results principally from interaction with a single state, then the first-order selection rules for perturbations [23] suggest that the perturber is a $^3\Pi_u$ state, interacting with $B^3\Sigma_u^-$ through the \mathcal{L} -uncoupling operator ($\Delta\Lambda = \Delta\Omega = \pm 1$). Only the $\Omega=0$ and $\Omega=2$ components of a $^3\Pi_u$ state with coupling approaching Hund's case (a) can produce a purely J -dependent interaction with $B^3\Sigma_{u1}^-(F_2, f)$ [4,24] and it is well known [24] that these components have completely different Λ -doubling characteristics, providing a possible explanation for the two classes of perturbation shown in Fig. 4. Using the more detailed arguments set out in the Appendix, we find that only the $\Omega=2$ component of the $^3\Pi_u$ perturber (small Λ doubling) can explain simultaneously the observed perturbation matrix ele-

ments for the F_2 and F_3 fine-structure components of $B(v=16)$, while only the $\Omega=0$ component (large Λ doubling) can explain the observed perturbations in the F_2 components of $B(v=17$ and $18)$ and the lack of perturbation of the nearby F_3 components.

It is advisable to consider whether a first-order picture of the perturbations is appropriate for the levels studied here. Near a dissociation limit, the separation in energy between electronic states can become small compared with the spin-orbit splittings, leading to a mixing of states with different Λ , Σ , and S values, and resulting in far-nuclei case (c) behavior [25] where only J and Ω are good quantum numbers. In the present case, the $B(16-18)$ levels lie $\sim 420-180 \text{ cm}^{-1}$ below the dissociation limit, respectively, while the off-diagonal spin-orbit interactions are expected to be less than the atomic spin-orbit parameter $\zeta_{\text{O}}(2p) = 150 \text{ cm}^{-1}$. Thus, a case (a) description of the perturber levels in this energy region is reasonable, but a description intermediate between cases (a) and (c) may be more appropriate for the perturbers of $B(v \geq 18)$.

B. Potential-energy curves

No Rydberg states of O_2 lie low enough in energy to produce bound-bound perturbations in $B^3\Sigma_u^-(v=16-18)$. However, the extensive *ab initio* calculations of Saxon and Liu [26] show several weakly bound *ungerade* valence states, correlating with the $\text{O}(^1D) + \text{O}(^3P)$ dissociation limit, some of which may be energetically capable of perturbing $B^3\Sigma_u^-(v=16-18)$. Since the first-order configuration-interaction (FOCI) calculations employed by Saxon and Liu [26] are expected to yield only qualitatively

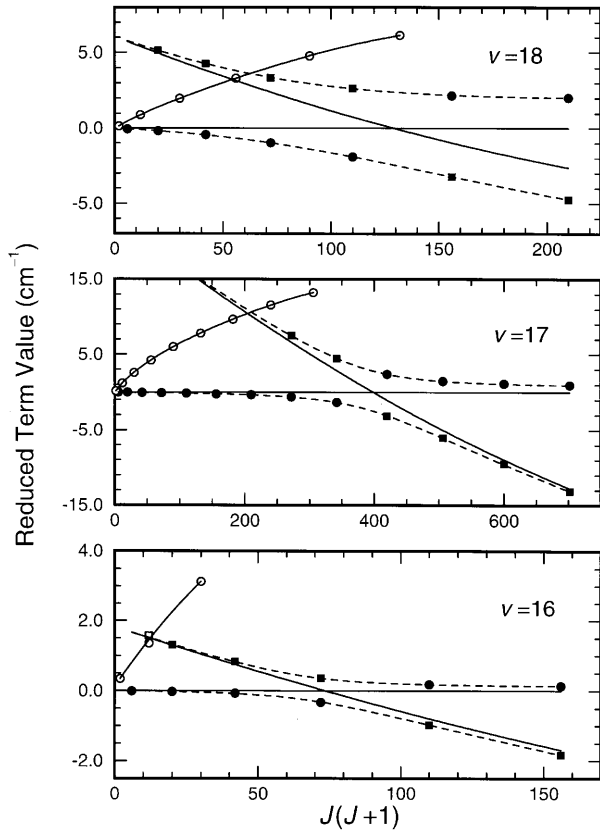


FIG. 4. Reduced term values for the main (circles) and extra (squares) levels associated with the lowest-energy rotational perturbations in the $F_2(f)$ (closed symbols) and $F_3(e)$ (open symbols) components of $B\ ^3\Sigma_u^-(v=16-18)$. Deperturbed energies of the respective F_2 levels (Table VII) have been subtracted from the absolute term values to enhance the visibility of the perturbations. The fitted perturbed (dashed lines) and deperturbed (solid lines) reduced term values were obtained using the two-level perturbation model described in the text and the respective model parameters given in Table VII. While the lowest-energy perturber level has closely spaced e - and f -parity components, resulting in a perturbation of $B\ ^3\Sigma_u^-(v=16, F_3)$, the F_3 levels for $v=17$ and 18 are unperturbed.

reliable binding energies for these states [6], we have performed MRCI + Q calculations according to the method described in Sec. IV, in order to assess more accurately the possible candidates for the perturbing state. Results for the three most strongly bound of these states are given in Table V. The corresponding potential-energy curves, formed by spline fitting the data of Table V and shifting in energy to be consistent with the experimental $O(^1D) + O(^3P)$ dissociation limit [27], are shown in Fig. 8. Spectroscopic constants, determined by fitting the G_v and B_v values obtained by numerical integration of the Schrödinger equation for these MRCI + Q potentials, are given in Table VI. The FO CI well depths calculated by Saxon and Liu [26] for these states exceed the MRCI + Q well depths by an average of 25%, somewhat less than, but in the same sense as, the discrepancy observed for other weakly bound states of O_2 correlating with the $O(^3P) + O(^3P)$ limit [6].

The MRCI + Q calculations, together with the evidence presented in Sec. V A, indicate that the second valence state

of ${}^3\Pi_u$ symmetry, which we name $C'\ ^3\Pi_u$, is responsible for the perturbations that we have observed in $B\ ^3\Sigma_u^-(v=16-18)$. As can be seen in Fig. 8, vibrational levels of the C' potential-energy curve occur near the $v=16-18$ levels of the B state and the C' - and B -state outer limbs are nearly coincident for $v \geq 18$, implying strong vibrational overlap. In addition, the large equilibrium internuclear distance for the C' potential ($R_e = 2.386$ Å) explains the lack of predissociation of this state: no repulsive states correlating with the only lower limit, $O(^3P) + O(^3P)$, rise rapidly enough to cross the bound portion of the C' state. Despite the fact that the $C'\ ^3\Pi_u \leftarrow X\ ^3\Sigma_u^-$ transition is electric-dipole allowed, very poor Franck-Condon overlap between the X state ($R_e = 1.208$ Å) and the C' state explains the negligible strength of the unperturbed $C' \leftarrow X$ lines.

Although ruled out as the principal perturber in a two-state interaction picture, it is possible that the $3\ ^3\Sigma_u^+$ and $2\ ^3\Delta_u$ states may produce other perturbations in the rotational structure of the B state. Energetically, the $3\ ^3\Sigma_u^+$ state could perturb $B(v \geq 18)$ through the first-order spin-orbit interaction ${}^3\Sigma_{u1}^+ - {}^3\Sigma_{u1}^-$, but such perturbations are likely to be weak, since, as can be seen in Fig. 8, the outer limbs of the potential-energy curves for the two states are well separated, implying small vibrational-overlap factors. Energetically, the $2\ ^3\Delta_u$ state could perturb $B(v \geq 16)$ through second-order interactions, principally of the type ${}^3\Sigma_u^- - {}^3\Pi_u - {}^3\Delta_u$, involving spin-orbit and/or \mathcal{L} -uncoupling interactions. These perturbations are also expected to be weak, not only because of their second-order nature, but also due to reasonably small vibrational-overlap factors. In addition, an examination of the calculated rotational constants in Table VI and those for the B -state levels in Table VII, indicates that such $2\ ^3\Delta_u$ perturbing levels would be likely to approach the perturbed levels from below, rather than above as is the case for the present observations. However, it is possible that some accidental perturbations involving coincidences between rovibrational levels of the B , C' , and $2\ ^3\Delta_u$ states will be observable. In fact, we have found some multiple perturbations, as yet unanalyzed, in rotational levels of $B\ ^3\Sigma_u^-(v \geq 16)$ higher than those discussed in this work. FO CI calculations [26] indicate that well depths for other weakly bound states correlating with the $O(^1D) + O(^3P)$ limit are < 100 cm^{-1} , implying that states other than the three discussed here are unlikely to play a role in the perturbation of $B\ ^3\Sigma_u^-(v \leq 20)$.

C. Deperturbation

We used a nonlinear least-squares fitting procedure and a simple two-level perturbation model [23] in which the unperturbed B - and C' -state term values were described by the usual polynomials in $J(J+1)$, with the additional assumption that the interaction matrix element was given by $|H_{BC'}| = |\eta_{BC'}| \sqrt{J(J+1) - \Omega_{C'}}$ (Fig. 7). For each level $B(v=16-18, F_2)$, we performed simultaneous fits to the measured main and extra term values listed in Tables I–III, respectively, and the width ratios $r = \Gamma_x/\Gamma_m$ listed in Table IV. The root-mean-square (RMS) term-value fitting deviations were only ~ 0.01 cm^{-1} , ~ 0.03 cm^{-1} , and ~ 0.02 cm^{-1} , respectively, for $v=16, 17$, and 18, supporting the high relative accuracy claimed for the measurements. The

TABLE IV. Measured upper-state predissociation linewidths and equivalent band oscillator strengths for $B^3\Sigma_u^-(v'=16-18, N', F_2$ and $F_3) \leftarrow X^3\Sigma_g^-(v''=0)$. Measured width ratios and energy separations for the main (m) and extra (x) levels observed in association with perturbations in $B^3\Sigma_u^-(v=16-18)$ are also shown, together with interaction matrix elements and level shifts estimated using Eqs. (5) and (6).

v'	Level	N'	$ T_m - T_x , \text{cm}^{-1}$	Γ_x/Γ_m	$\Gamma_m + \Gamma_x, \text{cm}^{-1}$	$(f_{v'm} + f_{v'x}) \times 10^5$	$ H_{mx} , \text{cm}^{-1}$	$ S , \text{cm}^{-1}$
16	F_2	2			0.343 ± 0.013	2.86 ± 0.09		
		4	1.33 ± 0.03	0.022 ± 0.008	0.362 ± 0.030	2.86 ± 0.30	0.191 ± 0.036	0.028 ± 0.011
		6	0.91 ± 0.02	0.095 ± 0.015	0.357 ± 0.017	2.80 ± 0.13	0.256 ± 0.017	0.079 ± 0.011
		8	0.69 ± 0.01	0.914 ± 0.063	0.316 ± 0.012	2.60 ± 0.09	0.345 ± 0.005	0.329 ± 0.013
		10	1.15 ± 0.01	0.181 ± 0.010	0.313 ± 0.005	2.61 ± 0.03	0.414 ± 0.010	0.176 ± 0.008
		12	1.96 ± 0.01	0.075 ± 0.009	0.299 ± 0.011	2.57 ± 0.08	0.499 ± 0.025	0.137 ± 0.015
		14			0.273 ± 0.011	2.44 ± 0.07		
		16			0.254 ± 0.006	2.34 ± 0.04		
		18			0.225 ± 0.008	2.14 ± 0.06		
		20			0.197 ± 0.014	1.98 ± 0.10		
16	F_3	2			0.36 ± 0.09	2.74 ± 0.39		
		4	0.22 ± 0.03	0.86 ± 0.22	0.38 ± 0.06	2.95 ± 0.40	0.110 ± 0.016	0.102 ± 0.022
		6			0.335 ± 0.025	2.89 ± 0.12		
		8			0.324 ± 0.016	2.83 ± 0.16		
		10			0.304 ± 0.005	2.66 ± 0.03		
		12			0.311 ± 0.010	2.70 ± 0.07		
		14			0.273 ± 0.010	2.55 ± 0.07		
		16			0.265 ± 0.007	2.37 ± 0.05		
		18			0.255 ± 0.010	2.25 ± 0.06		
		20			0.238 ± 0.023	2.13 ± 0.15		
17	F_2	2			0.281 ± 0.030	2.44 ± 0.17		
		4			0.286 ± 0.015	2.42 ± 0.10		
		6			0.278 ± 0.028	2.22 ± 0.19		
		8			0.280 ± 0.017	2.32 ± 0.11		
		10			0.294 ± 0.016	2.28 ± 0.09		
		12			0.286 ± 0.010	2.31 ± 0.08		
		14			0.245 ± 0.013	2.01 ± 0.08		
		16	8.12 ± 0.04	0.087 ± 0.008	0.219 ± 0.016	1.81 ± 0.14	2.20 ± 0.11	0.65 ± 0.06
		18	5.77 ± 0.04	0.281 ± 0.027	0.189 ± 0.008	1.49 ± 0.04	2.39 ± 0.10	1.27 ± 0.11
		20	5.45 ± 0.06	0.81 ± 0.10	0.108 ± 0.020	0.93 ± 0.12	2.71 ± 0.05	2.44 ± 0.16
		22	7.48 ± 0.04	0.245 ± 0.032	0.122 ± 0.024	1.30 ± 0.18	2.97 ± 0.12	1.47 ± 0.16
		24	10.65 ± 0.04	0.132 ± 0.013	0.115 ± 0.007	1.17 ± 0.03	3.42 ± 0.12	1.24 ± 0.11
26	14.06 ± 0.04	0.080 ± 0.012	0.088 ± 0.009	1.02 ± 0.05	3.68 ± 0.23	1.04 ± 0.14		
17	F_3	2			0.282 ± 0.102	2.24 ± 0.71		
		4			0.280 ± 0.036	2.48 ± 0.14		
		6			0.304 ± 0.032	2.32 ± 0.18		
		8			0.276 ± 0.012	2.38 ± 0.09		
		10			0.284 ± 0.009	2.31 ± 0.06		
		12			0.259 ± 0.010	2.11 ± 0.05		
		14			0.235 ± 0.010	2.12 ± 0.07		
		16			0.251 ± 0.014	2.01 ± 0.07		
18	F_2	2			0.207 ± 0.014	1.88 ± 0.09		
		4	5.32 ± 0.04	0.038 ± 0.009	0.198 ± 0.021	2.03 ± 0.09	1.00 ± 0.11	0.20 ± 0.05
		6	4.73 ± 0.05	0.10 ± 0.02	0.192 ± 0.029	1.75 ± 0.25	1.36 ± 0.12	0.43 ± 0.09
		8	4.33 ± 0.04	0.31 ± 0.03	0.159 ± 0.007	1.44 ± 0.04	1.84 ± 0.06	1.03 ± 0.09
		10	4.55 ± 0.04	0.70 ± 0.04	0.123 ± 0.009	1.05 ± 0.04	2.24 ± 0.03	1.87 ± 0.08
		12	5.41 ± 0.04	0.75 ± 0.08	0.118 ± 0.021	0.92 ± 0.08	2.68 ± 0.04	2.32 ± 0.15
		14	6.78 ± 0.04	0.47 ± 0.05	0.140 ± 0.011	1.07 ± 0.06	3.16 ± 0.08	2.17 ± 0.16

TABLE IV. (Continued).

v'	Level	N'	$ T_m - T_x , \text{cm}^{-1}$	Γ_x/Γ_m	$\Gamma_m + \Gamma_x, \text{cm}^{-1}$	$(f_{v'm} + f_{v'x}) \times 10^5$	$ H_{mx} , \text{cm}^{-1}$	$ S , \text{cm}^{-1}$
18	F_3	2			0.211 ± 0.027	1.94 ± 0.19		
		4			0.217 ± 0.017	1.87 ± 0.10		
		6			0.221 ± 0.009	2.02 ± 0.07		
		8			0.209 ± 0.010	2.03 ± 0.07		
		10			0.209 ± 0.009	1.91 ± 0.05		

fitted width ratios agreed with the measured values within the experimental uncertainties, except for $v=17, J=24$, where the deviation slightly exceeded the uncertainty. The deperturbed spectroscopic constants [28] obtained for the $B\ {}^3\Sigma_u^-$ - and $C'\ {}^3\Pi_u$ -state levels are given in Table VII, together with the fitted interaction matrix-element slopes $|\eta_{BC'}|$. The fitting procedure indicates that the perturbations for $B(16-18)$ culminate [23] at $J=8.1, J=19.5$, and $J=10.9$, respectively. The deperturbed term values, predissociation linewidths, and oscillator strengths consistent with the model parameters of Table VII, together with the fitted perturbed values, are shown in Figs. 4, 5, and 6, respectively.

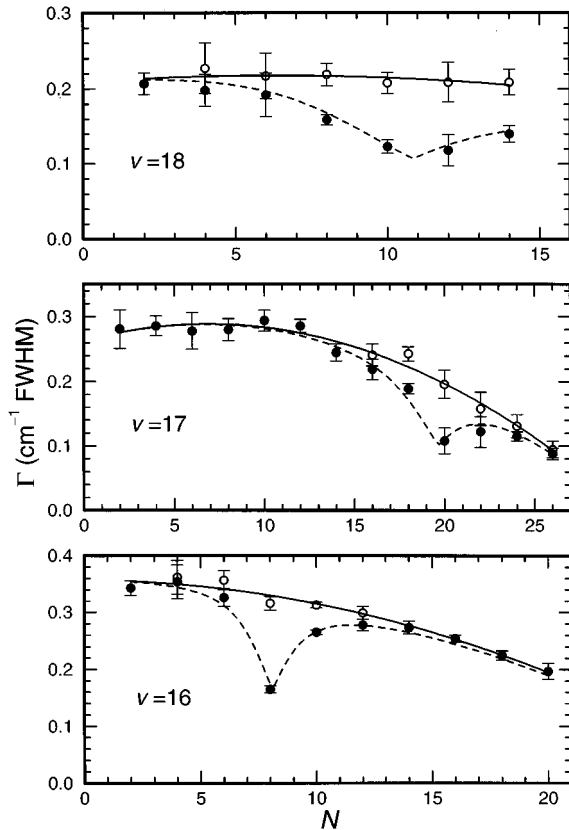


FIG. 5. Measured predissociation linewidths (closed circles) for the F_2 levels of $B\ {}^3\Sigma_u^-(v=16-18)$ in the region of their lowest-energy rotational perturbations. In the case of the perturbed levels, the sum of the linewidths for the main and extra lines (open circles) is also shown. The deperturbed linewidths (solid lines) were obtained from a quadratic fit to the main-extra linewidth sums, while the corresponding perturbed linewidths (dashed lines) were calculated using the two-level perturbation model described in the text and the respective model parameters given in Table VII.

In Fig. 7, the model interaction matrix elements are compared with the values determined individually from the measurements using Eq. (5). It is seen in all cases that the simple perturbation model which we have used gives an excellent description of the observations.

The best agreement between the calculated and deperturbed perturber levels is obtained by assuming that $C'(0)$ perturbs $B(16)$, $C'(2)$ perturbs $B(17)$, and $C'(3)$ perturbs $B(18)$. While these vibrational assignments are likely, they cannot be regarded as definitive until further experimental information on perturber isotope shifts becomes available.

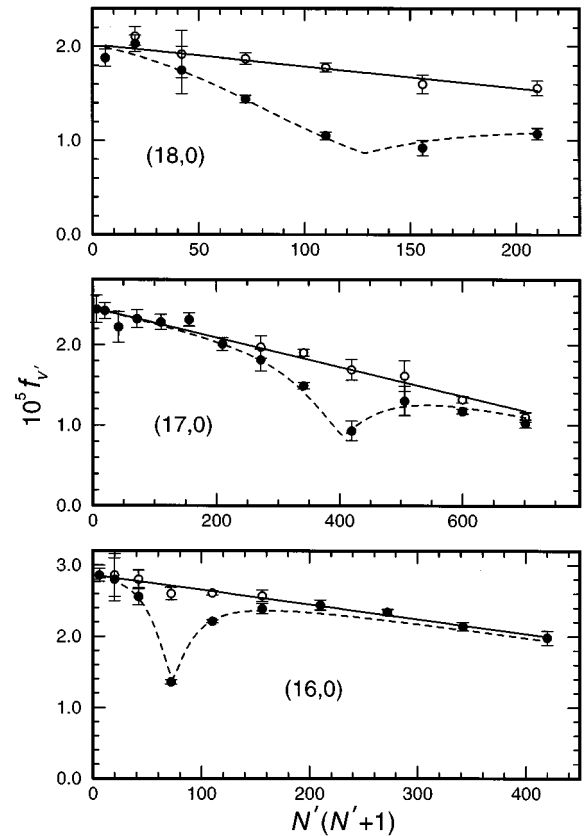


FIG. 6. Measured equivalent band oscillator strengths (closed circles) for the $B\ {}^3\Sigma_u^-(v=16-18, F_2) \leftarrow X\ {}^3\Sigma_g^-(v''=0)$ bands in the region of their lowest-energy rotational perturbations. In the case of the perturbed levels, the oscillator-strength sum for the main and extra lines (open circles) is also shown. The deperturbed oscillator strengths (solid lines) were obtained from a linear fit to the main-extra oscillator-strength sums, while the corresponding perturbed oscillator strengths (dashed lines) were calculated using the two-level perturbation model described in the text and the respective model parameters given in Table VII.

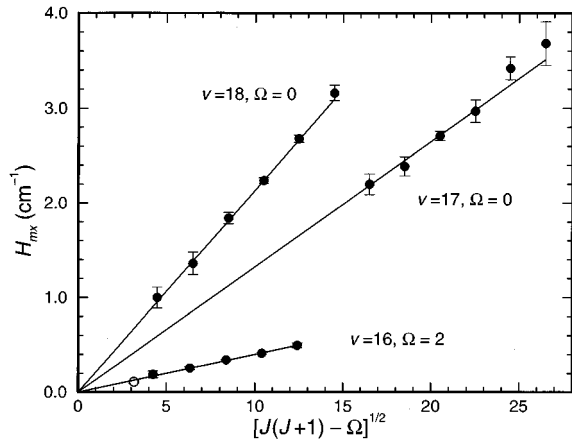


FIG. 7. Perturbation matrix elements for the interacting main and extra F_2 (closed circles) and F_3 (open circle) levels of $B\ ^3\Sigma_u^-(v=16-18)$, obtained from the measurements given in Table IV using Eq. (5). Fitted matrix elements (solid lines) implied by the respective two-level perturbation-model parameters given in Table VII are also shown. In anticipation of later conclusions in this work, and for consistency with expressions given in the Appendix, the abscissa of the figure includes the Ω value for the perturbing level, which differs for the $B(16)$ and $B(17$ and $18)$ perturbations, respectively.

Cheung *et al.* [10,12] have reported rotational perturbations in the $B(16)$ level of $^{16}\text{O}^{18}\text{O}$ and the $B(18)$ and $B(19)$ levels of $^{18}\text{O}_2$, but their failure to observe extra lines makes it difficult to determine the perturber origins for these isotomers. For comparative purposes, calculated MRCI + Q constants for the $C'\ ^3\Pi_u$ perturber levels are included in Table VII. The agreement between the deperturbed and calculated band origins and rotational constants is good, especially when it is realized that the calculated values do not take into account the spin-splitting of the $C'\ ^3\Pi_u$ state, and effectively refer to the $\Omega=1$ component, whereas the actual levels which perturb $B(16)$ and $B(17$ and $18)$ have $\Omega=2$ and $\Omega=0$, respectively. The calculated value of the centrifugal distortion constant D for the $C'(2)$ level agrees with the deperturbed value within the experimental uncertainty. However, since the $C'(3)$ level suffers a further perturbation from below for J values higher than those examined here, not removed by our two-level deperturbation procedure, the D value for this level is not fully deperturbed and cannot be compared with the calculated value.

The small discrepancies between the deperturbed and calculated perturber spectroscopic constants in Table VII can be reduced further by considering the spin-splitting of the $C'\ ^3\Pi_u$ state. It follows, approximately, from the triplet term formulas discussed by Kovács [24] that the origins of the outer components of a regular $^3\Pi$ term with coupling intermediate between Hund's cases (a) and (b) are given by $\nu_0 \pm A$, and the effective rotational constants by $B(1 \pm 2B/A)$, where ν_0 and B are the origin and rotational constant for the central component, $A > 0$ is the spin-orbit constant, and the upper and lower signs refer to the $\Omega=2$ and $\Omega=0$ components, respectively. Qualitatively, the application of these relations to the calculated $\Omega=1$ values in Table VII simultaneously increases the ν_0 and B values for $C'\ ^3\Pi_{u2}(v=0)$, while decreasing those for

TABLE V. Energies (in cm^{-1}), calculated at the MRCI + Q level, for three weakly bound states of O_2 correlating with the $\text{O}(^1D) + \text{O}(^3P)$ limit. Energies are referred to the $\text{O}(^3P) + \text{O}(^3P)$ limit.

R (a.u.)	$C'\ ^3\Pi_u$	$2\ ^3\Delta_u$	$3\ ^3\Sigma_u^+$
2.50		72827.54	
2.60		62190.18	
2.70		53250.23	80859.66
2.80		45817.28	68056.57
3.00	34170.16	34582.20	47896.91
3.20		26988.06	33595.93
3.25	27172.41		
3.40		22042.15	23487.62
3.50	21090.32		
3.60		17979.95	18897.54
3.75	17511.58		
3.80		16477.64	17120.72
4.00	16017.78	15758.97	16217.36
4.20		15490.76	15826.55
4.25	15540.28		
4.40		15447.00	15700.87
4.50	15454.00		
4.75	15490.94		
4.80		15575.29	15733.68
5.00	15556.66		
5.20		15719.54	15828.26
5.50	15679.83		
5.60		15815.67	15895.99
6.00	15771.80	15873.63	15936.25
6.50	15837.14	15915.26	
7.00	15882.77	15939.49	15976.41
7.50	15914.15	15954.84	15982.91
8.00	15935.53	15965.13	15986.18
9.00	15960.20	15976.85	15988.53
10.00	15966.93	15982.73	15989.28
11.00		15986.13	15989.86
100.0	15975.03		

$C'\ ^3\Pi_{u0}(v=2,3)$, providing better agreement with all of the deperturbed parameters. Quantitatively, invoking a regular $C'\ ^3\Pi_u$ state having a spin-orbit constant $A \approx +30\ \text{cm}^{-1}$ minimizes the discrepancies between the deperturbed and calculated origins and rotational constants. The verification of this tentative conclusion, however, must await the observation of more Ω levels of the C' state than those reported here.

We have estimated numerically the J -independent part of the \mathcal{L} -uncoupling interaction matrix elements between the RKR B -state potential and the calculated C' -state potential using Eq. (A3) with the electronic part replaced by the precession [23] value, i.e., $|\eta_{BC'}| = \sqrt{2}|\langle v_B | \mathcal{B} | v_{C'} \rangle|$. The vibrational quantum number of the C' state was treated as a continuous variable and the values of $|\eta_{BC'}|$ for levels degenerate with the B -state levels were estimated by graphical interpolation. Agreement between the relative calculated and deperturbed values, which is only fair, can be improved by considering the spin-structure of the C' state, as demonstrated above for the spectroscopic constants. For a regular

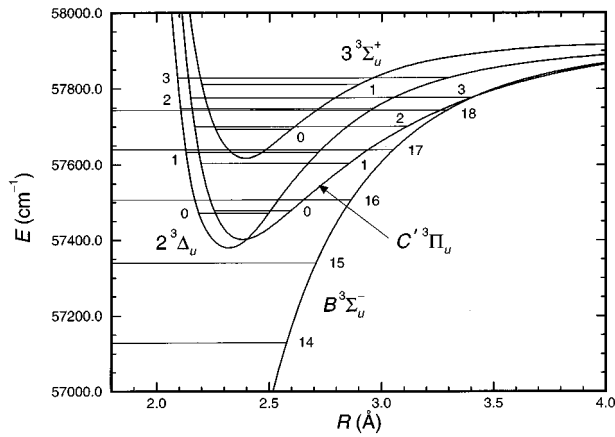


FIG. 8. Potential-energy curves for electronic states energetically capable of playing a role in the perturbation of $B^3\Sigma_u^-(v=16-18)$. The B -state curve is a RKR potential, while the others were obtained from spline fits to the MRCI + Q calculations of Table V, following shifting in energy to be consistent with the experimental $O(^1D) + O(^3P)$ dissociation limit [27]: the $C' {}^3\Pi_u$, $2 {}^3\Delta_u$, and $3 {}^3\Sigma_u^+$ curves were lowered by 106.5 cm^{-1} , 121.5 cm^{-1} , and 121.5 cm^{-1} , respectively. Energies are given relative to the minimum of the ground-state $X {}^3\Sigma_g^-$ potential-energy curve.

${}^3\Pi$ state, the effective potential-energy curves for the $\Omega=2$ and $\Omega=0$ components will lie a little above and below that for the $\Omega=1$ component, respectively, resulting in overlap factors $|\langle v_B | \mathcal{B} | v_{C'} \rangle|$ smaller for $\Omega=2$, and larger for $\Omega=0$, than those for $\Omega=1$. These variations are in such a sense as to improve agreement between the calculated and deperturbed relative values of $|\eta_{BC'}|$ given in Table VII. We do not pursue these considerations more quantitatively because of the great sensitivity of the overlap factors to the details of the calculated potential-energy curves, but merely note that the calculated MRCI + Q potential-energy curve for the C' state is broadly consistent with all of the deperturbed parameters of Table VII. In contrast, if, for example, we were to postulate that the level $B(18)$ were perturbed by either the $3 {}^3\Sigma_u^+$ or the $2 {}^3\Delta_u$ states, then the corresponding overlap factors result in numerical estimates of $|\eta|$ some 70 times and 15 times greater, respectively, than the tabulated value of $|\eta_{BC'}|$, clearly ruling out these states as the perturber.

Finally, from Tables I and IV, an estimate of the deperturbed term value for $C' {}^3\Pi_{u2}(v=0, J=3, e)$ of

$56\,725.72 \pm 0.04 \text{ cm}^{-1}$ can be determined. From our deperturbed spectroscopic constants for the C' state in Table VII, an estimated deperturbed term value for $C' {}^3\Pi_{u2}(v=0, J=3, f)$ of $56\,725.75 \pm 0.06 \text{ cm}^{-1}$ is obtained [29]. The deperturbed Λ doubling for $J=3$ is thus $T_f - T_e = 0.03 \pm 0.08 \approx 0 \text{ cm}^{-1}$ within the experimental uncertainty. As discussed in the Appendix, such a small value is consistent with expectation for a ${}^3\Pi_2$ level approaching Hund's coupling case (a).

D. Perturbations in λ_v and γ_v for $B^3\Sigma_u^-$

As noted in Sec. I, the spin-splitting constants for the $B^3\Sigma_u^-$ state of O_2 , λ_v and γ_v exhibit smooth perturbations which increase rapidly for high v as the B -state dissociation limit is approached. Bergeman and Wofsy [13] first suggested that the perturbation in λ_v could be explained by a spin-orbit interaction between the B state and a ${}^3\Pi_u$ state correlating with the same limit. Later, Julienne and Krauss [8] noted that the rotational constants B_v would also be affected by rotational interactions with such a ${}^3\Pi_u$ state, providing a possible explanation for the pathological turning in of the inner limbs of B -state RKR potential-energy curves derived from the experimental data. In this section, we investigate the consequences for λ_v and γ_v of the interactions between the $B^3\Sigma_u^-$ state and the $C' {}^3\Pi_u$ state, which, as we have seen in the previous sections, is responsible for rotational perturbations in the B -state levels with $v \geq 16$.

Brown *et al.* [31] have developed an effective Hamiltonian for diatomic molecules and give a convenient set of expressions for the R -dependent electronic Hamiltonian parameters which includes both direct contributions and the effects of interaction with other electronic states through appropriate perturbation-theory terms. For example, the effective spin-spin parameter $\lambda(R)$ comprises two contributions:

$$\lambda(R) = \lambda^{(1)}(R) + \lambda^{(2)}(R), \quad (7)$$

where $\lambda^{(1)}(R)$ results from the direct spin-spin interaction \mathcal{H}^{SS} and $\lambda^{(2)}(R)$ arises from second-order interactions involving the spin-orbit operator \mathcal{H}^{SO} . Thus, the effective spin-spin constant for the level v is given by

$$\lambda_v = \langle v | \lambda^{(1)}(R) | v \rangle + \langle v | \lambda^{(2)}(R) | v \rangle = \lambda_v^{(1)} + \lambda_v^{(2)}. \quad (8)$$

Field and Lefebvre-Brion [32] have estimated the direct component of λ_v for the B state of O_2 using the single-configuration approximation, obtaining $\lambda_v^{(1)} = 1.38 \text{ cm}^{-1}$. In

TABLE VI. Summary of spectroscopic constants for the three weakly bound states of Fig. 8 (in cm^{-1} , unless indicated otherwise), determined from fits to G_v and B_v values obtained by numerically integrating the Schrödinger equation for the MRCI + Q potential-energy curves of Fig. 8. Constants reproduce the G_v and B_v values to within $\pm 1 \text{ cm}^{-1}$ and $\pm 0.002 \text{ cm}^{-1}$, respectively.

State	T_e	D_e	ω_e	$\omega_e x_e$	$\omega_e y_e$	R_e (Å)	B_e	α_e	γ_e^a
$C' {}^3\Pi_u^b$	57406	518	154	16.0	0.63	2.386	0.370	0.0337	
$2 {}^3\Delta_u^c$	57372	552	211	27.0	1.12	2.301	0.398	0.0306	-0.0025
$3 {}^3\Sigma_u^+{}^d$	57621	303	158	20.9		2.401	0.366	0.0226	-0.0095

^aNot to be confused with the effective spin-rotation constant γ_v .

^bConstants determined from levels with $v=0-6$.

^cConstants determined from levels with $v=0-5$.

^dConstants determined from levels with $v=0-3$.

TABLE VII. Deperturbed spectroscopic constants and interaction matrix elements (in cm^{-1}) for levels of the $B\ ^3\Sigma_u^-$ and $C'\ ^3\Pi_u$ states, obtained from the measured term values of Tables I, II, and III and the width ratios of Table IV, together with comparable calculated constants for the $C'\ ^3\Pi_u$ levels.

State	Level	v	ν_0^a	B	$D \times 10^5$	$ \eta_{BC'} ^b$
$B\ ^3\Sigma_u^-$	F_2, f	16	56719.53 ± 0.03	0.3937 ± 0.0004	3.10 ± 0.08	
$C'\ ^3\Pi_u$	$\Omega = 2, f$	0 ^c	56721.35 ± 0.06	0.3670 ± 0.0015	~ 0.4	0.0402 ± 0.0012
$C'\ ^3\Pi_u$	$\Omega = 1, \text{calc.}^d$	0	56691.5	0.3545	0.94	0.05 ^e
$B\ ^3\Sigma_u^-$	F_2, f	17	56852.42 ± 0.06	0.3474 ± 0.0006	3.70 ± 0.01	
$C'\ ^3\Pi_u$	$\Omega = 0, f$	2 ^c	56875.65 ± 0.58	0.2808 ± 0.0026	1.4 ± 0.3	0.1325 ± 0.0022
$C'\ ^3\Pi_u$	$\Omega = 1, \text{calc.}^d$	2	56913.8	0.2852	1.63	0.09 ^e
$B\ ^3\Sigma_u^-$	F_2, f	18	56954.65 ± 0.06	0.3016 ± 0.0019	4.7 ± 1.0	
$C'\ ^3\Pi_u$	$\Omega = 0, f$	3 ^c	56960.70 ± 0.09	0.2460 ± 0.0024	-1.9 ± 1.1^f	0.2137 ± 0.0026
$C'\ ^3\Pi_u$	$\Omega = 1, \text{calc.}^d$	3	56988.5	0.2519	1.97	0.14 ^e

^aThe unperturbed B - and C' -state term values were represented by the polynomial $\nu_0 + BJ(J+1) - D[J(J+1)]^2$ in the deperturbation procedure.

^bThe interaction matrix elements are given by $|H_{BC'}| = |\eta_{BC'}| \sqrt{J(J+1) - \Omega_{C'}}$.

^cLikely vibrational numbering from *ab initio* calculations. Absolute numbering is not definitive.

^dConstants determined by numerical integration of the Schrödinger equation for the calculated C' potential-energy curve of Fig. 8.

^ePure-precession estimate $\sqrt{2} \langle v_B | \mathcal{B} | v_{C'} \rangle$ for degenerate levels.

^fAnomalous sign for D reflects a further perturbation at higher J , not included in the present analysis.

the unique-perturber approximation, where we assume that the B state is perturbed only by the C' state, the expression for the indirect contribution given by Brown *et al.* [31] reduces to

$$\lambda^{(2)}(R) = -\frac{1}{2} \frac{|\xi(R)|^2}{V_B(R) - V_{C'}(R)}, \quad (9)$$

where

$$\xi(R) = \langle B\ ^3\Sigma_{u1}^- | \mathcal{H}^{SO} | C'\ ^3\Pi_{u1} \rangle, \quad (10)$$

and $V_B(R)$ and $V_{C'}(R)$ represent the potential-energy curves of the B and C' states, respectively.

Similarly, the effective spin-rotation parameter $\gamma(R)$ is given by

$$\gamma(R) = \gamma^{(1)}(R) + \gamma^{(2)}(R), \quad (11)$$

where the first-order term $\gamma^{(1)}(R)$ results from the direct spin-rotation interaction \mathcal{H}^{SR} and is much smaller than the second-order term $\gamma^{(2)}(R)$ which arises from interactions with other states involving the product of the \mathcal{L} -uncoupling and spin-orbit operators. The effective spin-rotation constant for the level v is given by

$$\gamma_v = \langle v | \gamma^{(1)}(R) | v \rangle + \langle v | \gamma^{(2)}(R) | v \rangle = \gamma_v^{(1)} + \gamma_v^{(2)}. \quad (12)$$

With a unique-perturber view of the second-order contribution to the effective spin-rotation parameter of the B state, the expression given by Brown *et al.* [31] reduces to

$$\gamma^{(2)}(R) = -2\sqrt{2} \frac{\xi(R)\eta(R)}{V_B(R) - V_{C'}(R)}, \quad (13)$$

where

$$\eta(R) = \langle B\ ^3\Sigma_u^- | \mathcal{B} \mathcal{L}^- | C'\ ^3\Pi_u \rangle. \quad (14)$$

In principle, the sign of the interference cross-term $\xi(R)\eta(R)$ in Eq. (13), which is independent of the phase conventions for the molecular wave functions, can be determined experimentally by observing the sense of the perturbation in γ_v .

The expressions given by Julienne and Krauss [8] describing the perturbations in λ_v and γ_v for a $^3\Sigma$ state uniquely perturbed by a $^3\Pi$ state are equivalent to our treatment, but are computationally unattractive, involving perturbation sums over the discrete and continuum levels of the perturber. On the other hand, the expectation values of Eqs. (9) and (13) are easy to calculate and the resultant values of $\lambda_v^{(2)}$ and $\gamma_v^{(2)}$ should be accurate for levels in regions where the potential-energy curves of the B and C' states do not approach each other too closely. In this section, we consider only the B -state levels with $v \leq 15$. From Fig. 8, it can be seen that the separation in energy of the B - and C' -state potential-energy curves is $\sim 200\ \text{cm}^{-1}$ near the outer turning point for $B(v=15)$. As we shall see, this is significantly greater than the B - C' interaction matrix elements and implies that Eqs. (9) and (13) are applicable.

Effective values of λ_v and γ_v for B -state levels with $v=0-15$, determined from the measurements of Yoshino *et al.* [3] by Lewis *et al.* [33], are shown in Fig. 9, where the rapidly increasing perturbations for $v \geq 11$ can be seen readily. Using Eqs. (8), (9), (12), and (13), we have calculated values for $\lambda_v^{(2)}$ and $\gamma_v^{(2)}$ in the unique-perturber approximation. The RKR and calculated MRCI + Q potential-energy curves were used for $V_B(R)$ and $V_{C'}(R)$, respectively. In addition, it was assumed that $\xi(R)$ was R -independent [34] and that Eq. (14) could be rewritten as

$$\eta(R) = B(R)L^-(R), \quad (15)$$

where

$$B(R) = h/(8\pi^2\mu c R^2), \quad (16)$$

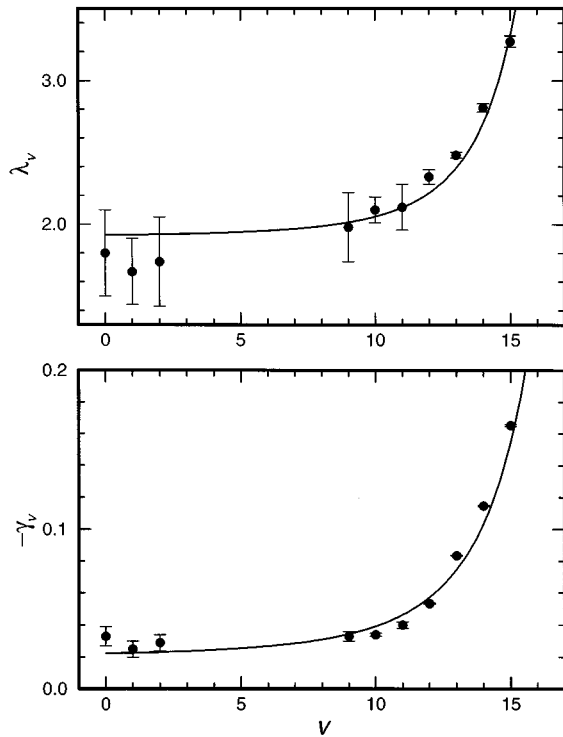


FIG. 9. Measured values (closed circles) of the spin-splitting parameters λ_v and γ_v for the $B\ {}^3\Sigma_u^-$ state, emphasizing the rapidly increasing perturbations for $v \geq 11$. Also shown are values of $1.8 + \lambda_v^{(2)}$ and $-0.015 + \gamma_v^{(2)}$ (lines) calculated in the unique-perturber approximation whereby it is assumed that only the $C'\ {}^3\Pi_u$ state perturbs the B state, and that the corresponding spin-orbit and L -uncoupling interactions are $\xi(R) = 35\text{ cm}^{-1}$ and $L^-(R) = -2.0$, respectively.

and

$$L^-(R) = \langle B\ {}^3\Sigma_u^- | L^- | C'\ {}^3\Pi_u \rangle \quad (17)$$

was also taken to be R -independent [34]. The results obtained with $\xi(R) = 35\text{ cm}^{-1}$, $L^-(R) = -2.0$ and constant effective values $\lambda_v^{(1)} = 1.8\text{ cm}^{-1}$ and $\gamma_v^{(1)} = -0.015\text{ cm}^{-1}$ are compared with the measurements in Fig. 9 where the agreement is seen to be very satisfactory. No allowance has been made for the small perturbations caused by the repulsive states, shown in Fig. 1, which are responsible for the B -state predissociation [8], but this will not affect our conclusions significantly. The character of the observed perturbations in λ_v and γ_v can be understood by referring to Fig. 8, where it can be seen that the energy denominator in Eqs. (9) and (13), $V_{C'}(R) - V_B(R)$, decreases for $R > R_e(C') = 2.39\text{ \AA}$, but increases very rapidly for $R < R_e$. Since the outer turning point for $B(v=12)$ is approximately equal to $R_e(C')$, this explains why the perturbations in the spin-splitting parameters have a rapid onset near $v = 12$.

Our value for $\xi(R)$ is in satisfactory agreement with values of 40 cm^{-1} and 32 cm^{-1} determined by Bergeman and Wofsy [13] and Cheung *et al.* [10], respectively, by fitting the perturbation in λ_v using a simple unique-perturber formula which did not involve the potential-energy curves of the relevant electronic states. A spin-orbit matrix element of this size seems reasonable: a value of 31 cm^{-1} has been

reported for the interaction between the B state and the first valence state of ${}^3\Pi_u$ symmetry [4]. There have been no previous estimates of $L^-(R)$.

As has been pointed out by Julienne and Krauss [8], whereas many electronic states can contribute to the perturbation of λ_v for the B state, only ${}^3\Pi_u$ states can contribute to the perturbation of γ_v (and B_v). The Wigner-Witmer correlation rules [35] imply that, in addition to the C' state, there are two other states of ${}^3\Pi_u$ symmetry associated with the $O({}^1D) + O({}^3P)$ limit. However, for the same electronic interaction strengths, our calculations show that these essentially repulsive states are expected to be 3–4 times less efficient than the C' state at perturbing the B state, due to greater separation in energy from the B -state potential. Of the other bound states shown in Fig. 8, only the $3\ {}^3\Sigma_u^+$ state has a first-order-allowed spin-orbit interaction with the B state, $\langle {}^3\Sigma_{u1}^+ | \mathcal{H}^{SO} | {}^3\Sigma_{u1}^- \rangle$, resulting in a perturbation which decreases λ_v . This is in the opposite sense to the perturbation produced by the C' state and observed experimentally, where both the $\Omega=0$ and $\Omega=1$ components participate in spin-orbit interactions in which the $B\ {}^3\Sigma_{u0}^-$ levels are depressed by twice as much as the $B\ {}^3\Sigma_{u1}^-$ levels. Julienne [9] has estimated a semiempirical spin-orbit matrix element of 16 cm^{-1} at $R = 2.117\text{ \AA}$ for the $3\ {}^3\Sigma_{u1}^+ - B\ {}^3\Sigma_{u1}^-$ interaction. If we adopt this value, together with our MRCI + Q potential-energy curve for the $3\ {}^3\Sigma_u^+$ state, then our estimate of the corresponding perturbation in λ_v is -15% of the observed value. Thus, the inclusion of this effect will change our conclusions only marginally. Despite all of the approximations in our analysis, it is likely that the interaction parameters obtained using the unique-perturber approximation will be qualitatively sound. Nevertheless, a complete *ab initio* study of the spin-orbit and L -uncoupling matrix elements between all relevant electronic states correlating with the $O({}^1D) + O({}^3P)$ limit would be invaluable in refining our picture of the B -state perturbation.

Summarizing the results of this section, we concur with the suggestion of Bergeman and Wofsy [13] that the perturbation in λ_v for the B state is caused principally by a single ${}^3\Pi_u$ state. Moreover, our unique-perturber calculations indicate that the perturbing state is likely to be the same $C'\ {}^3\Pi_u$ state that we have shown to be responsible for the rotational B -state perturbations reported in Sec. V A. The C' state is also principally responsible for the observed perturbations in γ_v . The negative sign determined for the electronic matrix-element product $L^-(R)\xi(R)$ is significant. In contrast, following a consideration of interference effects governing fine-structure-specific predissociation linewidths in the SR bands, Lewis *et al.* [4] found that the equivalent matrix-element product was positive for interactions between the B and $1\ {}^3\Pi_u$ states. Although there are significant uncertainties, adopting the calculated MRCI + Q potential-energy curve for the C' state, and considering both the analysis of observed rotational perturbations presented in Sec. V C and the results of this section, it appears that the magnitude of the J -independent part of the electronic L -uncoupling matrix element between the B and C' states is on the order of the pure-precession value $|L^-(R)| = \sqrt{2}$. This is not necessarily

to be expected for these mixed-configuration valence states [23] and suggests that an *ab initio* evaluation of this matrix element is desirable.

VI. CONCLUSIONS

Several rotational perturbations in the $B^3\Sigma_u^-$ state of molecular oxygen have been studied by measuring high-resolution VUV laser photoabsorption cross sections of the (16,0)–(18,0) Schumann-Runge bands of $^{16}\text{O}_2$. The observation of many extra lines in the spectrum, a line-profile analysis procedure which allows for non-Lorentzian line shapes due to interference between the main and extra lines, and state-of-the-art *ab initio* calculations have enabled the perturbing state to be identified as the second valence state of $^3\Pi_u$ symmetry, $C'^3\Pi_u$.

In particular, we have located three vibrational levels of the C' state which perturb $B(v=16-18, F_2)$ through an \mathcal{L} -uncoupling interaction. We have also shown that the C' state is likely to be responsible for much of the well-known rapid increase in the magnitudes of the B -state triplet-splitting constants λ_v and γ_v as the dissociation limit is approached.

Further work is in progress to examine and analyze other rotational perturbations in $B^3\Sigma_u^-(v \geq 16)$ which occur at higher energies, at higher rotational excitation, and in other fine-structure components. Eventually, with the aid of isotopic studies, we hope to make rigorous vibrational assignments and determine a realistic semiempirical potential-energy curve and spin-orbit constant for $C'^3\Pi_u$. In addition, it may be possible to clarify the roles of the $2^3\Delta_u$ and $3^3\Sigma_u^+$ states in the perturbation of the $B^3\Sigma_u^-$ state. *Ab initio* calculations of the spin-orbit and \mathcal{L} -uncoupling interactions between the $B^3\Sigma_u^-$ state and other states in this energy region would be extremely valuable in progressing towards a complete understanding of the $B^3\Sigma_u^-$ perturbations.

ACKNOWLEDGMENTS

The authors are grateful to Professor H. Lefebvre-Brion, Professor J. H. Carver, and Dr. L. W. Torop for critical comments on the manuscript. We also thank Professor M. L. Ginter for his assistance, comments, and suggestions made during visits to the ANU sponsored by the National Science Foundation (U.S.) through a U.S.-Australian Cooperative Research Grant. Valuable technical assistance was provided by K. J. Lonsdale and C. J. Dedman.

APPENDIX: THE $^3\Sigma_u^- - ^3\Pi_u$ COUPLING

$^3\Sigma - ^3\Pi$ perturbations have been discussed in detail by Kovács [24,36,37] and are central to an understanding of Λ doubling in $^3\Pi$ states [24,38]. Here, we are concerned primarily with determining which $^3\Pi_\Omega$ substates are responsible for the perturbations observed in the $F_2(v=16-18)$ and $F_3(v=16)$ levels of the $B^3\Sigma_u^-$ state.

If we express the molecular wave functions in the Hund's case (a) *e/f*-parity basis [23], then the nonzero $^3\Sigma - ^3\Pi$ interaction matrix elements are given by [4,8,39]

$$\langle ^3\Sigma_0^-, v, J, e | \mathcal{H} | ^3\Pi_0, v', J, e \rangle = \sqrt{2}(\xi + \sqrt{2}\eta), \quad (\text{A1a})$$

$$\langle ^3\Sigma_0^-, v, J, e | \mathcal{H} | ^3\Pi_1, v', J, e \rangle = -\eta\sqrt{2J(J+1)}, \quad (\text{A1b})$$

$$\langle ^3\Sigma_1^-, v, J, f | \mathcal{H} | ^3\Pi_0, v', J, f \rangle = \mp \eta\sqrt{J(J+1)}, \quad (\text{A1c})$$

$$\langle ^3\Sigma_1^-, v, J, f | \mathcal{H} | ^3\Pi_1, v', J, f \rangle = \xi + \sqrt{2}\eta, \quad (\text{A1d})$$

$$\langle ^3\Sigma_1^-, v, J, f | \mathcal{H} | ^3\Pi_2, v', J, f \rangle = -\eta\sqrt{J(J+1)-2}, \quad (\text{A1e})$$

where

$$\xi(v, v', J) = \langle v, J | \langle ^3\Sigma_1^- | \mathcal{H}^{SO} | ^3\Pi_1 \rangle | v', J \rangle, \quad (\text{A2})$$

$$\eta(v, v', J) = \langle v, J | \langle ^3\Sigma^- | \mathcal{B}\mathcal{L}^- | ^3\Pi \rangle | v', J \rangle, \quad (\text{A3})$$

and \mathcal{H} , \mathcal{H}^{SO} , and $\mathcal{B}\mathcal{L}^-$ represent the full molecular Hamiltonian, the spin-orbit operator, and the J -independent part of the \mathcal{L} -uncoupling operator, respectively.

Over the full range of rotation, appropriate wave functions for the $B^3\Sigma_u^-$ state are intermediate between Hund's coupling cases (a) and (b) and can be expressed as [40,41]

$$|^3\Sigma_u^-, F_1, v, J \rangle = a|^3\Sigma_0^-, v, J, e \rangle + b|^3\Sigma_1^-, v, J, e \rangle, \quad (\text{A4a})$$

$$|^3\Sigma_u^-, F_2, v, J \rangle = |^3\Sigma_1^-, v, J, f \rangle, \quad (\text{A4b})$$

$$|^3\Sigma_u^-, F_3, v, J \rangle = b|^3\Sigma_0^-, v, J, e \rangle - a|^3\Sigma_1^-, v, J, e \rangle. \quad (\text{A4c})$$

The mixing parameters a and b are given by

$$a(v, J) = \sqrt{[T_2(v, J) - T_1(v, J)]/[T_3(v, J) - T_1(v, J)]}, \quad (\text{A5a})$$

$$b(v, J) = \sqrt{[T_3(v, J) - T_2(v, J)]/[T_3(v, J) - T_1(v, J)]}, \quad (\text{A5b})$$

where $T_i(v, J)$ are the fine-structure term values, provided that centrifugal distortion is neglected [40].

First, we wish to consider the interactions of the F_2 levels of the B state. From Eqs. (A1c), (A1e) and (A4b), it can be seen that only the $^3\Pi_0$ and $^3\Pi_2$ substates can interact with a $^3\Sigma_1^-$ state in a way consistent with the J -dependent perturbation matrix element measured in this work. From Eqs. (A1) and (A4), the interactions of these $^3\Pi_{u\Omega}$ substates with $B^3\Sigma_u^-(F_2)$ and F_3 are given by

$$\langle ^3\Sigma_u^-, F_2, v, J | \mathcal{H} | ^3\Pi_{u0}, v', J, f \rangle = \eta\sqrt{J(J+1)}, \quad (\text{A6a})$$

$$\begin{aligned} \langle ^3\Sigma_u^-, F_3, v, J | \mathcal{H} | ^3\Pi_{u0}, v', J, e \rangle &= \sqrt{2}b(\xi + \sqrt{2}\eta) \\ &\quad + a\eta\sqrt{J(J+1)}, \end{aligned} \quad (\text{A6b})$$

and

$$\langle {}^3\Sigma_u^-, F_2, v, J | \mathcal{H} | {}^3\Pi_{u2}, v', J, f \rangle = -\eta\sqrt{J(J+1)-2}, \quad (A7a)$$

$$\langle {}^3\Sigma_u^-, F_3, v, J | \mathcal{H} | {}^3\Pi_{u2}, v', J, e \rangle = a\eta\sqrt{J(J+1)-2}. \quad (A7b)$$

In the case of $B\ {}^3\Sigma_u^-(v=16, J=3)$, substituting into Eq. (A5) the deperturbed term values $T_3(16,3)$ deduced from Tables I and IV, $T_2(16,3)$ deduced from Table VII, and the unperturbed $T_1(16,3)$ of Yoshino *et al.* [3], we find that $a(16,3)=0.92$ and $b(16,3)=0.38$. If the perturbing substate is ${}^3\Pi_{u0}$, from Eq. (A6) the ratio of the F_3 and F_2 perturbation matrix elements is

$$\frac{H_3(v, J)}{H_2(v, J)} = a + \frac{\sqrt{2}b(\xi + \sqrt{2}\eta)}{\eta\sqrt{J(J+1)}}. \quad (A8)$$

Thus, $H_3(16,3)/H_2(16,3) \approx 0.92 + 0.155\xi/\eta$, assuming that $\eta \ll \xi$. With this assumption, the second term (of either sign) will dominate and the ratio will be much greater than unity, inconsistent with our observations. For example, in the case of the interaction between the B state and the $1\ {}^3\Pi_u$ valence state, it has been reported by Lewis *et al.* [4] that $\eta/\xi=0.019$. In this case, $H_3(16,3)/H_2(16,3) \approx 9$. However, if the perturbing substate is ${}^3\Pi_{u2}$, from Eq. (A7) it follows that $H_3(v, J)/H_2(v, J) = -a$ and $H_3(16,3)/H_2(16,3) = -0.92$. Clearly, this is consistent with our observation, illustrated in Fig. 7, that $|H_3(16,3)/H_2(16,3)| \approx 1$ and demonstrates that the perturber of $B(16)$ is a ${}^3\Pi_{u2}$ state.

The above arguments, based on a case (a) picture of the ${}^3\Pi_u$ perturber, are essentially unchanged when we consider a ${}^3\Pi_u$ state with coupling intermediate between cases (a) and (b), but tending to case (a). This situation is expected to apply for rotational quantum numbers $J \ll Y = A/B$, where A and B are the diagonal spin-orbit and rotational constants of the ${}^3\Pi_u$ state, respectively. Applying this approximation to the triplet transformation matrix of Kovács [24], we can express the intermediate-coupled ${}^3\Pi_u$ wave functions in terms of the case (a) basis functions as follows:

$$|{}^3\Pi_{u0}', v, J\rangle \approx |{}^3\Pi_{u0}, v, J\rangle + \frac{\sqrt{2J(J+1)}}{Y} |{}^3\Pi_{u1}, v, J\rangle, \quad (A9a)$$

$$|{}^3\Pi_{u1}', v, J\rangle \approx -\frac{(J-1)\sqrt{2(J+1)}}{Y\sqrt{J}} |{}^3\Pi_{u0}, v, J\rangle + |{}^3\Pi_{u1}, v, J\rangle + \frac{J\sqrt{2(J+2)}}{Y\sqrt{(J-1)}} |{}^3\Pi_{u2}, v, J\rangle, \quad (A9b)$$

$$|{}^3\Pi_{u2}', v, J\rangle \approx -\frac{\sqrt{2(J-1)(J+2)}}{Y} |{}^3\Pi_{u1}, v, J\rangle + |{}^3\Pi_{u2}, v, J\rangle. \quad (A9c)$$

Using Eqs. (A9a) and (A9c), it is easy to show that the form of Eqs. (A6a) and (A7a) remains unchanged when the ${}^3\Pi_u$

state has intermediate coupling with $J \ll Y$, but the parameter η must be replaced by an effective value given by $\eta_{\text{eff}} \approx \eta + \sqrt{2}\xi/(Y\eta)$. In other words, the conclusion that only ${}^3\Pi_{u2}$ or ${}^3\Pi_{u0}$ states can produce purely J -dependent perturbations in the F_2 levels of the B state remains valid for coupling intermediate between cases (a) and (b), but tending to case (a). Thus, the observation that the experimental perturbation matrix elements shown in Fig. 7 do not deviate significantly from a linear J dependence for $J \lesssim 25$ implies that the value of Y for the perturber is significantly greater than 25. Similarly, although Eqs. (A6b) and (A7b) are slightly modified in the case of intermediate coupling, both by the appearance of terms weakly dependent on J^2 and by the introduction of effective values for η in the J -dependent terms, the conclusion, based on a consideration of the ratio $H_3(16,3)/H_2(16,3)$, that the perturber of $B(16)$ is a ${}^3\Pi_{u2}$ state remains valid.

Support for these conclusions can be obtained from a consideration of Λ doubling in ${}^3\Pi$ states. For a ${}^3\Pi$ state conforming to Hund's case (a) coupling ($Y \rightarrow \infty$), the Λ -doubling expressions given by Brown and Merer [38] reduce to

$$\Delta T_{fe}({}^3\Pi_0) = 2(o_v + p_v + q_v), \quad (A10a)$$

$$\Delta T_{fe}({}^3\Pi_1) = q_v J(J+1), \quad (A10b)$$

$$\Delta T_{fe}({}^3\Pi_2) = 0, \quad (A10c)$$

where o_v , p_v , and q_v are the normal Λ -doubling parameters [31,38]. The parameter o_v includes the effect of the direct spin-spin interaction and the effects of spin-orbit interactions with other electronic states. The second-order parameters q_v and p_v represent the effects of interactions with other states through the \mathcal{L} -uncoupling operator, and through the product of the \mathcal{L} -uncoupling and spin-orbit operators, respectively. Broadly speaking, the Λ -doubling parameters for a ${}^3\Pi$ state embody the same interactions as those responsible for the perturbations in λ_v , γ_v , and B_v for a ${}^3\Sigma$ state and mathematical inter-relationships can be demonstrated in the case of the unique-perturber approximation and further simplifying assumptions [38].

An examination of Eq. (A10) indicates that the Λ -doubling characteristics for the ${}^3\Pi_0$ and ${}^3\Pi_2$ components differ considerably. The lack of doubling expected for a ${}^3\Pi_2$ level supports the classification of the $B(16)$ perturber as a ${}^3\Pi_{u2}$ level, since an inspection of Fig. 4 shows minimal splitting between the e and f levels of this perturber. The nonzero doubling expected for a ${}^3\Pi_0$ level is consistent with the classification of the $B(17)$ and $B(18)$ perturbers as ${}^3\Pi_{u0}$ levels, since we have observed no e -level perturbers for these B -state levels, implying that the Λ doubling in these cases is large, i.e., beyond the scale of Fig. 4. This can be understood by anticipating the results of Sec. V D in which it is proposed that the B state and the perturbing ${}^3\Pi_u$ state are in a unique-perturber relationship, resulting in large pertur-

bations in λ_v for the B -state levels with $v \geq 17$. Under these conditions, it is expected that the magnitude of σ_v will be dominated by this unique spin-orbit interaction, and that the e levels of the ${}^3\Pi_{u0}$ perturber will be pushed to energies

significantly higher than the corresponding f levels, since the B state has no $\Omega=0$ levels of f parity. This expectation is consistent with the lack of perturbation of the $F_3(e)$ levels of $B(v=17$ and $18)$ shown in Fig. 4.

-
- [1] M. Nicolet and P. Mange, *J. Geophys. Res.* **59**, 15 (1954).
- [2] M. Nicolet, *J. Geophys. Res.* **89**, 2573 (1984).
- [3] K. Yoshino, D. E. Freeman, and W. H. Parkinson, *J. Phys. Chem. Ref. Data* **13**, 207 (1984).
- [4] B. R. Lewis, S. T. Gibson, and P. M. Dooley, *J. Chem. Phys.* **100**, 7012 (1994).
- [5] B. R. Lewis, L. Berzins, J. H. Carver, and S. T. Gibson, *J. Quant. Spectrosc. Radiat. Transfer* **36**, 187 (1986).
- [6] H. Partridge, C. W. Bauschlicher, S. R. Langhoff, and P. R. Taylor, *J. Chem. Phys.* **95**, 8292 (1991).
- [7] H. Partridge (unpublished).
- [8] P. S. Julienne and M. Krauss, *J. Mol. Spectrosc.* **56**, 270 (1975).
- [9] P. S. Julienne, *J. Mol. Spectrosc.* **63**, 60 (1976).
- [10] A. S.-C. Cheung, K. Yoshino, D. E. Freeman, R. S. Friedman, A. Dalgarno, and W. H. Parkinson, *J. Mol. Spectrosc.* **134**, 362 (1989).
- [11] P. Brix and G. Herzberg, *Can. J. Phys.* **32**, 110 (1954).
- [12] A. S.-C. Cheung, K. Yoshino, D. E. Freeman, and W. H. Parkinson, *J. Mol. Spectrosc.* **131**, 96 (1988).
- [13] T. H. Bergeman and S. C. Wofsy, *Chem. Phys. Lett.* **15**, 104 (1972).
- [14] R. N. Zare, A. L. Schmeltekopf, W. J. Harrop, and D. L. Albritton, *J. Mol. Spectrosc.* **46**, 37 (1973).
- [15] B. R. Lewis, J. P. England, R. J. Winkel, Jr., S. S. Banerjee, P. M. Dooley, S. T. Gibson, and K. G. H. Baldwin, *Phys. Rev. A* **52**, 2717 (1995).
- [16] R. Hilbig and R. Wallenstein, *IEEE J. Quantum Electron.* **QE-19**, 194 (1983).
- [17] K. Yamanouchi and S. Tsuchiya, *J. Phys. B* **28**, 133 (1995).
- [18] The VUV bandwidth was found to be sensitive to the dye-laser pulse energies and the details of the dye-laser oscillator setup procedures. In normal operation, the pulse energies were reduced until the observed linewidths became constant, and temporal variations in bandwidth were monitored by the repeated measurement of a narrow reference line.
- [19] L. Veseth and A. Lofthus, *Mol. Phys.* **27**, 511 (1974).
- [20] B. R. Lewis, P. M. Dooley, J. P. England, S. T. Gibson, K. G. H. Baldwin, and L. W. Torop (unpublished).
- [21] J. Almlöf and P. R. Taylor, *J. Chem. Phys.* **86**, 4070 (1987).
- [22] The subscript x indicates an extra line associated with a transition into the perturbing state: for example, $P_{3,x}(5)$ refers to the extra line which perturbs the main line $P_3(5)$.
- [23] H. Lefebvre-Brion and R. W. Field, *Perturbations in the Spectra of Diatomic Molecules* (Academic, Orlando, 1986), pp. 39, 51–58, 196–197, 226–231, 247–248.
- [24] I. Kovács, *Rotational Structure in the Spectra of Diatomic Molecules* (Hilger, London, 1969), pp. 68–70, 76–79, 258–261.
- [25] R. S. Mulliken, *Rev. Mod. Phys.* **3**, 89 (1931).
- [26] R. P. Saxon and B. Liu, *J. Chem. Phys.* **67**, 5432 (1977).
- [27] S. T. Gibson, B. R. Lewis, K. G. H. Baldwin, and J. H. Carver, *J. Chem. Phys.* **94**, 1060 (1991).
- [28] Due to the fragmentary observations of the C' -state levels, we used the simple polynomial form $\nu_0 + BJ(J+1) - D[J(J+1)]^2$ to describe the unperturbed term values of the B and C' states. Thus, our deperturbed band origins will be defined differently from those obtained using a full molecular Hamiltonian in the deperturbation procedure.
- [29] The deperturbed term value for $C' {}^3\Pi_{u2}(J=3, f)$ must be estimated since this is a virtual level. In the case of a homonuclear molecule with nuclear spin $I=0$, such as ${}^{16}\text{O}_2$, the odd- J levels of a ${}^3\Pi_{u2}(f)$ state have zero statistical weight [30].
- [30] G. Herzberg, *Molecular Spectra and Molecular Structure I. Spectra of Diatomic Molecules* (Van Nostrand, New York, 1950), pp. 133–140.
- [31] J. M. Brown, E. A. Colbourn, J. K. G. Watson, and F. D. Wayne, *J. Mol. Spectrosc.* **74**, 294 (1979).
- [32] R. W. Field and H. Lefebvre-Brion, *Acta Phys. Hung.* **35**, 51 (1974).
- [33] B. R. Lewis, L. Berzins, and J. H. Carver, *J. Quant. Spectrosc. Radiat. Transfer* **36**, 209 (1986).
- [34] The assumption of R -independent off-diagonal matrix elements between the B and C' states may not be very good due to R -dependent configuration mixing.
- [35] E. Wigner and E. E. Witmer, *Z. Phys.* **51**, 859 (1928).
- [36] I. Kovács, *Z. Phys.* **111**, 640 (1939).
- [37] I. Kovács, *Can. J. Phys.* **36**, 309 (1958).
- [38] J. M. Brown and A. J. Merer, *J. Mol. Spectrosc.* **74**, 488 (1979).
- [39] K. F. Freed, *J. Chem. Phys.* **45**, 4214 (1966).
- [40] J. K. G. Watson, *Can. J. Phys.* **46**, 1637 (1968).
- [41] J. B. Tatum and J. K. G. Watson, *Can. J. Phys.* **49**, 2693 (1971).